International Journal of Heat and Mass Transfer 205 (2023) 123919

Contents lists available at ScienceDirect

International Journal of Heat and Mass Transfer

journal homepage: www.elsevier.com/locate/hmt

Analysis of a diffusion-reaction heat transfer problem in a finite thickness layer adjoined by a semi-infinite medium

Ankur Jain

Mechanical and Aerospace Engineering Department, University of Texas at Arlington, 500W First St, Rm 211, Arlington, TX 76019, USA

ARTICLE INFO

Article history:
Received 8 November 2022
Revised 1 January 2023
Accepted 28 January 2023

Keywords:
Thermal runaway
Semi-infinite body
Laplace transforms
Li-ion cells
Semiconductor devices

ABSTRACT

Multilayer diffusion-reaction problems are of much interest for both heat and mass transfer. While past work in this direction has mainly addressed multilayer bodies of finite size, practical problems such as immersion cooling of Li-ion cells and thermal runaway in semiconductor devices necessitate considering one of the layers to be semi-infinite. This work presents theoretical analysis of a diffusion-reaction problem in a finite layer surrounded by an infinite medium on both sides, where heat generation proportional to the local temperature occurs in the finite layer. Transient temperature distributions in the two bodies are determined using Laplace transformation technique. Through analysis of the poles of the solution in the Laplace domain, it is proved that this problem is unconditionally unstable, in that temperature in the finite thickness layer is predicted to always diverge at large times. However, the time taken to reach the unstable regime is shown to depend strongly on the key non-dimensional parameters of the problem. Temperature in the finite layer is shown to exhibit non-monotonic behavior at small times, particularly for large values of the heat generation coefficient, which is explained on the basis of the balance between temperature-dependent heat generation, heat dissipation into the semi-infinite medium and eventual slowdown of heat dissipation due to temperature rise. The impact of thermal properties on thermal behavior of the system is examined. A practical problem related to thermal safety design of a Li-ion cell is solved. Results from this work expand the state-of-the-art in theoretical analysis of diffusion-reaction problems, and also offer practical tools for thermal design of engineering problems including Li-ion cells and semiconductor devices.

1. Introduction

Heat transfer in multilayer bodies is of much theoretical and practical interest in a variety of engineering problems, including thermal property measurements [1,2], thermal management [3], building insulation [4], thin films [5] and structural engineering [6]. Theoretical analysis of one-dimensional diffusion-based transport in a multilayer body of finite thickness is usually carried out using the separation of variables method [7], wherein the quasi-orthogonality of eigenfunctions [8] plays a key role. Problems with complications such as time-dependent [9] or spatially-varying [10] boundary conditions have also been solved using variants of this technique. A combination of separation of variables and Laplace transformation techniques has also been used [11]. A number of numerical techniques have also been used for solving multilayer thermal conduction problems [12,13].

Diffusion-reaction problems form an important subset of multilayer thermal conduction problems. Such problems are relevant when temperature-dependent heat generation occurs in one or more layers, for example, Arrhenius heat generation due to chemical reaction in Li-ion cells [14], and Joule heating in a Metal–Oxide–Semiconductor Field-Effect Transistor (MOSFET) with temperature-dependent current characteristics [15]. In the context of mass transfer, reactions that generate or consume species also result in a diffusion-reaction problem [16,17]. In such cases, linearization of the generation term results in an additional term in the energy/species conservation equation, requiring somewhat more complicated analysis. Multilayer diffusion-reaction problems have been solved using the separation of variables method, where quasi-orthogonality of eigenfunctions has been shown to be unaffected by the generation term [18]. More complicated problems, such as multilayer convection-diffusion-reaction (CDR) problems have also been solved [19].

Convergence and stability are of much importance in diffusion-reaction problems due to the positive feedback between temperature rise and heat generation. In short, heat generation results in temperature rise, which, due to the temperature-dependent heat generation term, results in greater heat generation and further temperature rise. In the absence of sufficient heat dissipa-

E-mail address: jaina@uta.edu

https://doi.org/10.1016/j.ijheatmasstransfer.2023.123919
0017-9310/

Nomenclature

k	thermal conductivity ($Wm^{-1}K^{-1}$)
L	half thickness of the finite layer (m)
T	temperature (K)
x	spatial coordinate (m)
t	time (s)
α	thermal diffusivity (m^2s^{-1})
$\bar{\alpha}_2$	non-dimensional thermal diffusivity, $\bar{\alpha}_2 = \frac{\alpha_2}{\alpha_1}$
$\bar{k}_2$	non-dimensional thermal conductivity, $\bar{k}_2 = \frac{k_2}{k_1}$
τ	non-dimensional time, $\tau = \frac{\alpha_1 t}{L^2}$
θ_i	non-dimensional temperature, $\theta_i = \frac{T_i - T_0}{T_{in} - T_0}$ (i=1, 2)
$\hat{\theta}_i$	Laplace transform of temperature (i=1, 2)
ξ	non-dimensional spatial coordinate, $\xi = \frac{x}{L}$
Subscripts	
0	ambient
1	finite layer
2	semi-infinite medium
max	maximum value
in	initial

tion driven by diffusion within the body and convection on the boundaries, this may lead to a thermal runaway situation, as is well-known to occur in Li-ion cells [14] and in MOSFET devices [20]. Analytical solutions for specific thermal runaway problems are available [14,21]. It has been shown that one or more eigenvalues in a multilayer finite-thickness diffusion-reaction problem may be imaginary [18,22], which leads to divergence in temperature at large times. Closed-form expressions for the threshold conditions for thermal runaway to occur [14,18], as well as the number of imaginary eigenvalues [22] have been derived.

The literature discussed above mostly addresses the diffusion-reaction problem in finite bodies. In contrast, diffusion-reaction may also be of interest when a finite thickness body is surrounded by an infinite external medium, as shown schematically in Fig. 1(a). In case heat generation in a finite thickness body is temperature-dependent, it is unclear whether heat dissipation into the infinite medium may be sufficient to prevent thermal runaway. One practical problem where such a scenario may be encountered is in the cooling of a thin prismatic Li-ion cell immersed in a large stationary fluid, where heat generation in the cell due to decomposition reactions may be approximated, to the first degree, by a heat generation term that rises linearly with temperature [14]. Another relevant example is related to heat dissipation from a thin MOSFET into the surrounding substrate [20]. In this case, heat generation in the MOSFET can increase with increasing temperature due to temperature-dependent current characteristics [15]. The substrate is located on only one side of the MOSFET in traditional semi-

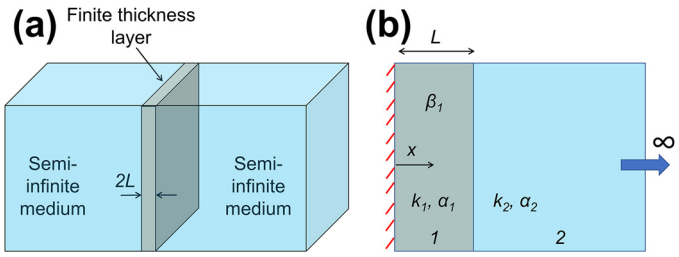

Fig. 1. Schematics showing (a) the geometry of a finite body of thickness 2*L* in an infinite medium; (b) details of the half-geometry considered in this work based on symmetry.

conductor devices, whereas, more recently, 3D integrated circuits (3D ICs) [23], particularly monolithic 3D ICs [24], result in the substrate being on both sides of the MOSFET. In both of the examples cited above, it is of interest to determine whether the temperature field diverges at large times or not. Interesting physical phenomena that occur in such a problem include heat generation in the finite body, which is expected to increases as the finite body gets hotter and cooling due to conduction into the infinite medium, which is expected to slow down over time due to temperature rise in the semi-infinite medium.

A robust mathematical model is needed for developing a fundamental understanding of these phenomena and their trade-offs with each other. While much work already exists on analysis of diffusion-reaction problems in finite multilayer bodies, there is a lack of work in scenarios where one of the bodies is semi-infinitely large. The limited work available on heat transfer between a finite layer and a semi-infinite medium [7,25] mostly presents only pure-diffusion analysis, which does not account for temperature-dependent heat generation. The usual separation of variables technique that has been used successfully for finite thickness problems cannot be used in this case since the quasi-orthogonality of eigenfunctions is not valid in a semi-infinite geometry. An alternate technique is needed for addressing the important questions posed above.

This work presents a Laplace transforms based analysis of a two-layer diffusion-reaction problem, in which, a finite layer with temperature-dependent heat generation is adjoined by a semi-infinite body. A solution for the problem is derived in the Laplace domain, which is then inverted numerically. Analysis of the poles of the solution in Laplace domain is carried out to prove that this problem is unconditionally unstable. Results are shown to correctly reduce to past work for the special case of a pure-diffusion problem. Results are also shown to be in good agreement with finite-element simulations. The dependence of the nature of the temperature field on the rate of change of heat generation with temperature as well as other problem parameters such as thermal properties is investigated. Applications of these results exist in stability analysis of Li-ion cells and semiconductor devices.

2. Problem definition

Fig. 1(a) presents a schematic of the problem under consideration here. A one-dimensional body of thickness 2*L* is submerged in an infinitely large, stationary medium on both sides. Internal heat generation occurs within the finite body at a rate that is proportional to the local temperature. Heat generated in the finite body is conducted into the infinite medium. The temperature-dependent heat generation modeled in this problem may represent, for example, exothermic heat generation in a Li-ion cell due to electrochemical decomposition reactions, or Joule heating in a semiconductor MOSFET with a temperature-dependent current, whereas the infinite medium may represent, for example, a dielectric coolant fluid in the battery problem, and the Silicon substrate surrounding the MOSFET in the semiconductor problem [20]. The semi-infinite medium is assumed to be stationary, with no convective heat transfer within. In the context of immersion cooling of a Li-ion cell, this implies that the coolant fluid is not being circulated.

By symmetry, only one half of the problem may be modeled, as shown in Fig. 1(b), in which, the geometry comprises a finite layer of thickness L in contact with a semi-infinite layer. Thermal conductivity and diffusivity are denoted by k and α, respectively, and subscripts *1* and *2* denote the finite layer and semi-infinite medium, respectively. The semi-infinite medium is assumed to be at ambient temperature T_0 initially, while a uniform initial temperature $T_{in}(> T_0)$ is assumed for the finite layer. Perfect thermal contact between the two is assumed. All properties are assumed

to be uniform and independent of temperature. Dimensions in the directions normal to the x direction as shown in Fig. 1(b) are assumed to be large enough to enable treating thermal conduction to be one-dimensional in nature. Based on these assumptions, the energy conservation equations that govern the temperature fields $T_1(x,t)$ and $T_2(x,t)$ in the finite layer and semi-infinite medium, respectively, may be written as follows:

$$\alpha_1 \frac{\partial^2 T_1}{\partial x^2} + \beta_1 T_1 = \frac{\partial T_1}{\partial t} \qquad (0 < x < L) \tag{1}$$

$$\alpha_2 \frac{\partial^2 T_2}{\partial x^2} = \frac{\partial T_2}{\partial t} \qquad (x > L) \tag{2}$$

where, $\beta_1 > 0$ is the linear heat generation coefficient that connects heat generation in the finite layer to the local temperature.

Boundary conditions associated with this problem may be written as follows:

$$\frac{\partial T_1}{\partial x} = 0 \qquad (x = 0) \tag{3}$$

$$T_1 = T_2 \qquad (x = L) \tag{4}$$

$$k_1 \frac{\partial T_1}{\partial x} = k_2 \frac{\partial T_2}{\partial x} \qquad (x = L) \tag{5}$$

$$T_2 \to T_0 \qquad (x \to \infty) \tag{6}$$

Here, Eq. (3) is due to symmetry considerations along the center of the finite layer, Eqs. (4) and (5) model perfect thermal contact and heat flux conservation, respectively, at the interface, and Eq. (6) arises from the semi-infinite nature of the surrounding medium.

The initial condition associated with this problem is

$$T_1 = T_{in};\ T_2 = T_0 \qquad (t = 0) \tag{7}$$

3. Derivation of the solution

In order to solve the problem defined by Eqs. (1)–(7), it is helpful to carry out a non-dimensionalization first. Doing so reduces the number of parameters of the problem, helps identify important non-dimensional groups governing the solution of the problem and facilitates parametric analysis. The following non-dimensional variables are introduced:

$$\theta_1 = \frac{T_1 - T_0}{T_{in} - T_0},\ \theta_2 = \frac{T_2 - T_0}{T_{in} - T_0},\ \xi = \frac{x}{L},\ \tau = \frac{\alpha_1 t}{L^2},\ \bar{\alpha}_2 = \frac{\alpha_2}{\alpha_1},$$
$$\bar{k}_2 = \frac{k_2}{k_1},\ \bar{\beta}_1 = \beta_1 L^2/\alpha_1 \tag{8}$$

Note that $\bar{\beta}_1$ represents the strength of the generation term relative to the diffusion term. The other two non-dimensional parameters that appear are the ratios of thermal conductivity and thermal diffusivity. Based on the non-dimensionalization outlined above, the following non-dimensional equations and associated boundary/initial conditions may be written

$$\frac{\partial^2 \theta_1}{\partial \xi^2} + \bar{\beta}_1 \theta_1 = \frac{\partial \theta_1}{\partial \tau} \qquad (0 < \xi < 1) \tag{9}$$

$$\frac{\partial^2 \theta_2}{\partial \xi^2} = \frac{1}{\bar{\alpha}_2} \frac{\partial \theta_2}{\partial \tau} \qquad (\xi > 1) \tag{10}$$

$$\frac{\partial \theta_1}{\partial \xi} = 0 \qquad (\xi = 0) \tag{11}$$

$$\theta_1 = \theta_2 \qquad (\xi = 1) \tag{12}$$

$$\frac{\partial \theta_1}{\partial \xi} = \bar{k}_2 \frac{\partial \theta_2}{\partial \xi} \qquad (\xi = 1) \tag{13}$$

$$\theta_2 \to 0 \qquad (\xi \to \infty) \tag{14}$$

$$\theta_1 = 1;\ \theta_2 = 0 \qquad (\tau = 0) \tag{15}$$

It is of interest to solve this non-dimensional problem to investigate whether heat absorption in the semi-infinite body is able to keep the temperature of the finite layer from diverging at large times due to the positive feedback between temperature and heat generation.

Note that in case both layers are finite in dimension, the resulting two-layer diffusion-reaction problem has already been solved using the separation of variables method, and conditions for divergence have been derived explicitly [18,22]. However, in the present case, this is not possible due to the semi-infinite nature of the second body, which precludes the use of an eigenfunction-based solution. A special case of the present problem with no temperature-dependent heat generation, which makes this a pure-diffusion problem, has been solved using Laplace transforms technique [7]. After deriving a solution for the problem in the Laplace domain, it has been shown that an analytical inversion results in a solution comprising error functions. Therefore, the Laplace transforms technique is also used for solving the present problem. In general, the Laplace transformation involves appropriate integration of the governing equations over time, which introduces a new Laplace variable, but removes time dependence, thereby resulting in significant simplification. This makes it possible to derive an explicit solution of the problem in the Laplace domain. Laplace transformation technique is commonly used for solving thermal conduction and other engineering problems [7].

Carrying out Laplace transform of Eqs. (9) and (10) while making use of the initial condition given by Eq. (15) results in

$$\hat{\theta}_1'' + \bar{\beta}_1 \hat{\theta}_1 = s\hat{\theta}_1 - 1 \qquad (0 < \xi < 1) \tag{16}$$

$$\hat{\theta}_2'' = \frac{s}{\bar{\alpha}_2} \hat{\theta}_2 \qquad (\xi > 1) \tag{17}$$

where, $\hat{}$ represents the Laplace transform, and s is the Laplace variable.

Eqs. (16) and (17) can be solved easily as follows:

$$\hat{\theta}_1(\xi, s) = -\frac{1}{\gamma_1^2} + A_1 \cos(\gamma_1 \xi) + B_1 \sin(\gamma_1 \xi) \qquad (0 < \xi < 1) \tag{18}$$

$$\hat{\theta}_2(\xi, s) = A_2 \exp(\gamma_2 \xi) + B_2 \exp(-\gamma_2 \xi) \qquad (\xi > 1) \tag{19}$$

where, $\gamma_1 = \sqrt{\bar{\beta}_1 - s}$ and $\gamma_2 = \sqrt{s/\bar{\alpha}_2}$.

Based on Laplace transforms of boundary conditions given by Eqs. (11) and (14), $B_1 = 0$ and $A_2 = 0$, respectively. Moreover, using the Laplace transforms of interface conditions given by Eqs. (12) and (13), one may write

$$\frac{1}{\gamma_1^2} + A_1 \cos(\gamma_1) = B_2 \exp(-\gamma_2) \tag{20}$$

$$-\gamma_1 A_1 \sin(\gamma_1) = -\bar{k}_2 \gamma_2 B_2 \exp(-\gamma_2) \tag{21}$$

A_1 and B_2 may be determined by solving the linear equations given by Eqs. (20) and (21). The subsequent solution for the temperature fields in the Laplace domain is found to be

$$\hat{\theta}_1(\xi, s) = \frac{1}{\gamma_1^2}\left(-1 + \frac{\cos(\gamma_1 \xi)}{\cos(\gamma_1) - \frac{\gamma_1}{\bar{k}_2 \gamma_2} \sin(\gamma_1)}\right) \qquad (0 < \xi < 1) \tag{22}$$

$$\hat{\theta}_2(\xi,s)=\frac{\exp\left(\gamma_2(1-\xi)\right)}{\cos\left(\gamma_1\right)-\frac{\gamma_1}{\bar{k}_2\gamma_2}\sin\left(\gamma_1\right)}\cdot\frac{\sin\left(\gamma_1\right)}{\gamma_1\bar{k}_2\gamma_2}\qquad(\xi>1)\quad(23)$$

which completes the solution for the problem in the Laplace domain. For the special case of $\bar{\beta}_1=0$, it can be shown that Eqs. (22) and (23) correctly reduce to the results presented before for the pure-diffusion problem [7]. While an explicit inversion was carried out for the pure-diffusion problem, in the present case, due to the considerable complication in Eqs. (18) and (19) from the temperature-dependent heat generation term, an explicit inversion is unlikely to be possible. However, a number of numerical inversion techniques are available [26,27]. In the present work, the de Hoog quotient difference method algorithm [26] is used to determine the temperature fields in the two layers.

4. Stability analysis

Due to the presence of both temperature-dependent heat generation and cooling due to heat dissipation into the semi-infinite medium, it is unclear without further analysis whether the solution derived in Section 3 results in a stable or unstable temperature distribution. In particular, due to the positive feedback ($\bar{\beta}_1>0$) between temperature rise and heat generation rate in the finite layer, it is of interest to determine if the semi-infinite medium is able to sufficiently dissipate heat and keep the temperature field $\theta_1(\xi,\tau)$ bounded at large times.

In order to do so, the nature of the solution in the Laplace domain, $\hat{\theta}_1(\xi,s)$, is examined. In particular, it is well known from linear stability theory [28] that a function $f(t)$ diverges at large time if its Laplace transform $\hat{f}(s)$ has at least one pole with a positive real component. Further, a function $\hat{f}(s)=\frac{p(s)}{q(s)}$ has a pole of order 1 at $s=s_0$ if and only if the following conditions apply [29]: (1) $q(s_0)=0$, (2) $q'(s_0)\neq 0$, (3) $p(s_0)\neq 0$, and (4) both p and q are analytic at $s=s_0$.

For the solution derived for $\hat{\theta}_1(\xi,s)$ in Section 3, given by Eq. (22), one may write

$$p(\xi,s)=\frac{\sin\left(\gamma_1\right)}{\bar{k}_2\gamma_1\gamma_2}+\frac{\cos\left(\gamma_1\xi\right)-\cos\left(\gamma_1\right)}{\gamma_1^2}\qquad(24)$$

$$q(s)=\cos\left(\gamma_1\right)-\frac{\gamma_1\sin\left(\gamma_1\right)}{\bar{k}_2\gamma_2}\qquad(25)$$

Based on these expressions, it is proved in the following subsections that $\hat{\theta}_1(\xi,s)$ satisfies each of the conditions listed above at at least one point in the range $0<s<\bar{\beta}_1$, thus proving the existence of at least one real positive pole for $\hat{\theta}_1(\xi,s)$. Once this is established, it clearly follows that temperature distribution in the finite layer diverges unconditionally at large times.

4.1. Proof that $q(s)$ has at least one root in $0<s<\bar{\beta}_1$

In order to show that $q(s)$ has at least one root in $0<s<\bar{\beta}_1$, the values of $q(s)$ approaching the two ends of this range are examined. For $s\to 0^+$, one may obtain $\gamma_1\to\sqrt{\bar{\beta}_1}$ and $\gamma_2\to 0^+$. Therefore, $q(s)\to 1-\frac{\sqrt{\bar{\beta}_1}\sin(\sqrt{\bar{\beta}_1})}{\bar{k}_2\ \gamma_2}$. If $\bar{\beta}_1<\pi^2/4$, this implies that $q(s)\to-\infty$ as $s\to 0^+$. On the other hand, at $s=\bar{\beta}_1$, one may obtain $\gamma_1=0$ and $\gamma_2=\sqrt{\bar{\beta}_1/\bar{\alpha}_2}$, and thus, $q(s)=1$ at $s=\bar{\beta}_1$. Further, Section 4.1.1 below proves that $q(s)$ is a continuous function in this range. Since $q(s)$ begins at $-\infty$ at the start of the range, becomes positive at the end of the range and is a continuous function throughout, therefore, $q(s)$ must cross the s axis at least once within this range, i.e., must have at least one root in $0<s<\bar{\beta}_1$.

This is illustrated in Fig. 2(a), which presents plots of $q(s)$ for multiple values of $\bar{\beta}_1$ with $\bar{\alpha}_2=2.0$ and $\bar{k}_2=3.0$. In each case, as expected, $q(s)$ has a large negative value as $s\to 0^+$ and a value of 1 at the other end of the range, and, therefore, is seen to cross the x axis in each case.

4.1.1. Proof that $q(s)$ is a continuous function throughout $0\le s<\bar{\beta}_1$

Clearly, $q(s)$ is well defined in $0<s<\bar{\beta}_1$, as given by Eq. (25). Further, at any point $s=s_0$ in this range,

$$\lim_{s\to s_0}q(s)=\lim_{s\to s_0}\cos\left(\sqrt{\bar{\beta}_1-s}\right)-\frac{\sqrt{\bar{\alpha}_2}}{\bar{k}_2}\lim_{s\to s_0}\sin\left(\sqrt{\bar{\beta}_1-s}\right)\sqrt{\frac{\bar{\beta}_1}{s}-1}\qquad(26)$$

Since the limit of a product of two functions is the product of the limits of the two functions, and since $s_0\neq 0$, one may obtain

$$\lim_{s\to s_0}q(s)=\cos\left(\sqrt{\bar{\beta}_1-s_0}\right)-\frac{\sqrt{\bar{\alpha}_2}}{\bar{k}_2}\sin\left(\sqrt{\bar{\beta}_1-s_0}\right)\sqrt{\frac{\bar{\beta}_1}{s_0}-1}=q(s_0)\qquad(27)$$

This applies for both left and right side limits. Therefore, the limit of $q(s)$ at any point in $0<s<\bar{\beta}_1$ is equal to its value at that point. This shows that $q(s)$ is a continuous function in $0<s<\bar{\beta}_1$.

4.2. Proof that $q'(s)\neq 0$ throughout $0\le s<\bar{\beta}_1$

By differentiating Eq. (25), one may write

$$q'(s)=\frac{\sin\left(\gamma_1\right)}{2\gamma_1}+\frac{1}{\bar{k}_2}\frac{\sin\left(\gamma_1\right)+\gamma_1\cos\left(\gamma_1\right)}{2\gamma_1\gamma_2}+\frac{\gamma_1\sin\left(\gamma_1\right)}{2\gamma_2 s}\qquad(28)$$

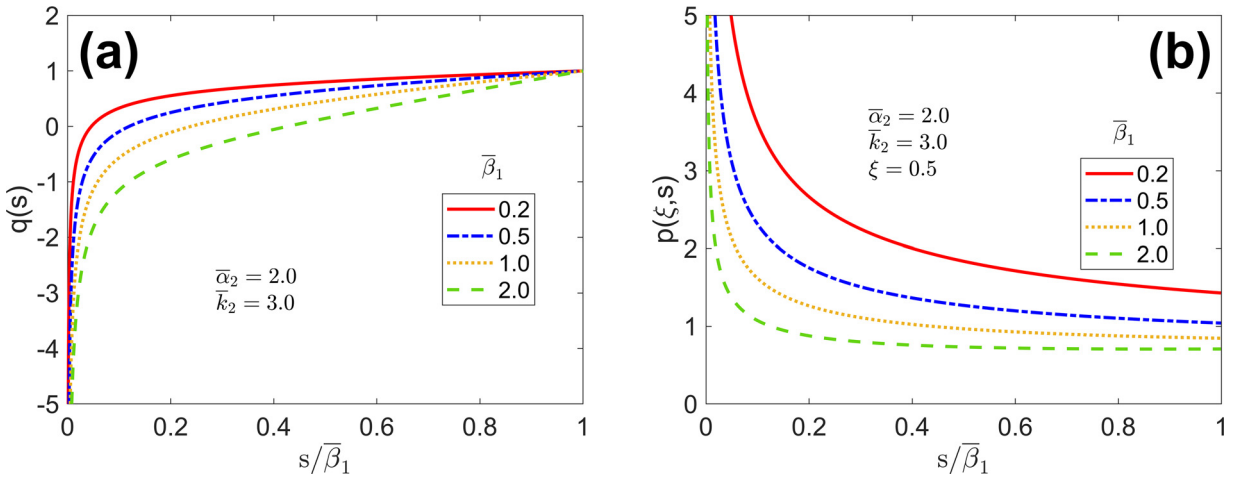

Fig. 2. Plots of functions (a) $q(s)$, and (b) $p(\xi,s)$ for multiple values of $\bar{\beta}_1$. Problem parameters are $\bar{\alpha}_2=2$, $\bar{k}_2=3$. For $p(s)$, $\xi=0.5$ is used.

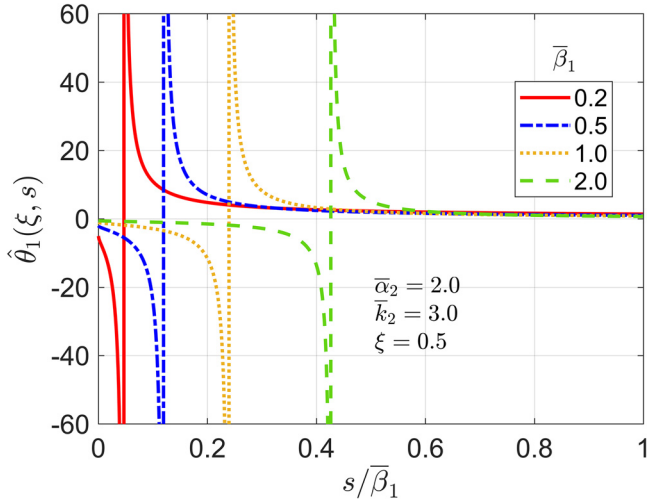

Fig. 3. Plot of $\hat{\theta}_1(\xi, s)$ as a function of s in the range $0 < s < \bar{\beta}_1$ for multiple values of $\bar{\beta}_1$. Other problem parameters are $\bar{\alpha}_2 = 2$, $\bar{k}_2 = 3$, $\xi = 0.5$.

Now, for $\bar{\beta}_1 < \pi^2/4$, each of the terms in Eq. (28) above are positive, and, therefore, $q'(s)$ is positive throughout the range $0 < s < \bar{\beta}_1$.

4.3. Proof that $p(s) \neq 0$ throughout $0 \leq s < \bar{\beta}_1$

As $s \to 0^+$, $\gamma_1 \to \sqrt{\bar{\beta}_1}$ and $\gamma_2 \to 0^+$. At the other end of the range, at $s = \bar{\beta}_1$, $\gamma_1 = 0$ and $\gamma_2 = \sqrt{\bar{\beta}_1/\bar{\alpha}_2}$. Both γ_1 and γ_2 remain positive in this range. Further, $\sin(\gamma_1) > 0$ if $\bar{\beta}_1 < \pi^2/4$, since $\gamma_1 < \sqrt{\bar{\beta}_1}$. Therefore, the first term in the expression for $p(s)$ given by Eq. (24) is positive. As for the remaining two terms, from the above conditions, $\gamma_1 < \pi/2$, and, therefore, $\cos(\gamma_1 \xi) > \cos(\gamma_1)$, since $\xi < 1$ in the finite layer and cosine is a decreasing function between 0 and $\pi/2$. Therefore, the sum of second and third terms in Eq. (24) is also positive. Therefore, it follows that $p(s)$ is positive throughout $0 < s < \bar{\beta}_1$ for all values of $\xi < 1$, if $\bar{\beta}_1 < \pi^2/4$.

This result is illustrated in Fig. 2(b), which presents plots of $p(\xi, s)$ for multiple values of $\bar{\beta}_1$, with $\bar{\alpha}_2 = 2$, $\bar{k}_2 = 3$, $\xi = 0.5$. These plots show that for each value of $\bar{\beta}_1$ considered in this Figure, $p(\xi, s)$ remains positive throughout $0 < s < \bar{\beta}_1$, as established by the proof above.

4.4. Proof that $p(s)$ and $q(s)$ are both analytic throughout $0 \leq s < \bar{\beta}_1$

Both p and q comprise functions that are individually analytic. Therefore, p and q are also analytic in the range considered here.

Taken together, the proofs presented above establish that the finite layer temperature in the Laplace domain, $\hat{\theta}_1(\xi, s)$, has at least one real positive pole of order 1 when $\bar{\beta}_1 < \pi^2/4$. Therefore, the temperature distribution in the finite layer diverges at large times, and the problem considered in this work is unconditionally unstable.

Note that each proof in Sections 4.1–4.3 is valid only for $\bar{\beta}_1 < \pi^2/4$. It can be argued that if the problem is unconditionally unstable in this range, then increasing $\bar{\beta}_1$ beyond $\pi^2/4$ will not remove the instability since a larger $\bar{\beta}_1$ results in an even stronger positive feedback between heat generation and temperature, thereby moving the problem even more towards instability. Therefore, while proved specifically for $\bar{\beta}_1 < \pi^2/4$, the conclusion of unconditional instability is true for all positive values of $\bar{\beta}_1$.

As an illustration, Fig. 3 plots $\hat{\theta}_1(\xi, s)$ as a function of s for $\xi = 0.5$, $\bar{\alpha}_2 = 2.0$ and $\bar{k}_2 = 3.0$ for four different values of $\bar{\beta}_1$. It is found that in each case, the function exhibits a pole at a positive value of s smaller than $\bar{\beta}_1$, as predicted by the proofs discussed above. Further, the locations of the poles for the four curves in Fig. 3 correspond exactly with the zeroes of the corresponding plots of $q(s)$ shown in Fig. 2(a).

Note that the derivation presented in this section does not place any limitations on the other two parameters of the problem, $\bar{\alpha}_2$ and $\bar{k}_2$, or on the location ξ within the finite layer. Therefore, the results are valid everywhere in the finite layer and for all values of thermal properties of the materials.

5. Results and discussion

5.1. Comparison with past work and numerical simulations

The present work generalizes past work on pure diffusion analysis in a stack of a finite thickness layer and a semi-infinite medium [7] by accounting for temperature-dependent heat generation in the finite layer. Therefore, it is instructive to compare results from the present work with pure-diffusion results. This comparison is presented in Fig. 4, where Fig. 4(a) presents a plot of temperature at $\xi = 0.5$ in the center of the finite

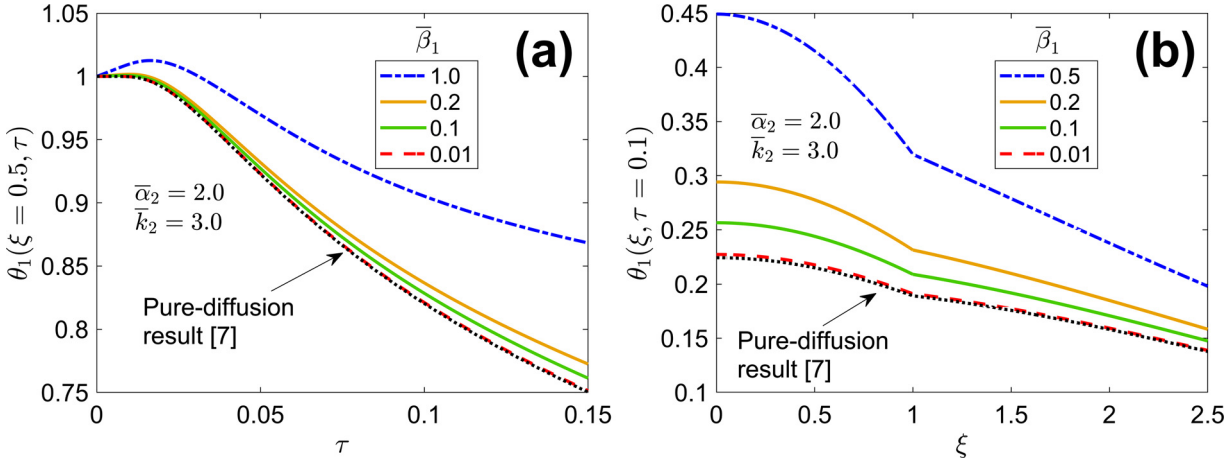

Fig. 4. Verification of the solution technique: (a) temperature at the center of finite layer as a function of time, and (b) temperature distribution at $\tau = 2.0$. In both cases, curves corresponding to multiple values of $\bar{\beta}_1$ based on the present work are plotted. For comparison, pure-diffusion results from past work [7] are also plotted. Problem parameters are $\bar{\alpha}_2 = 2$, $\bar{k}_2 = 3$.

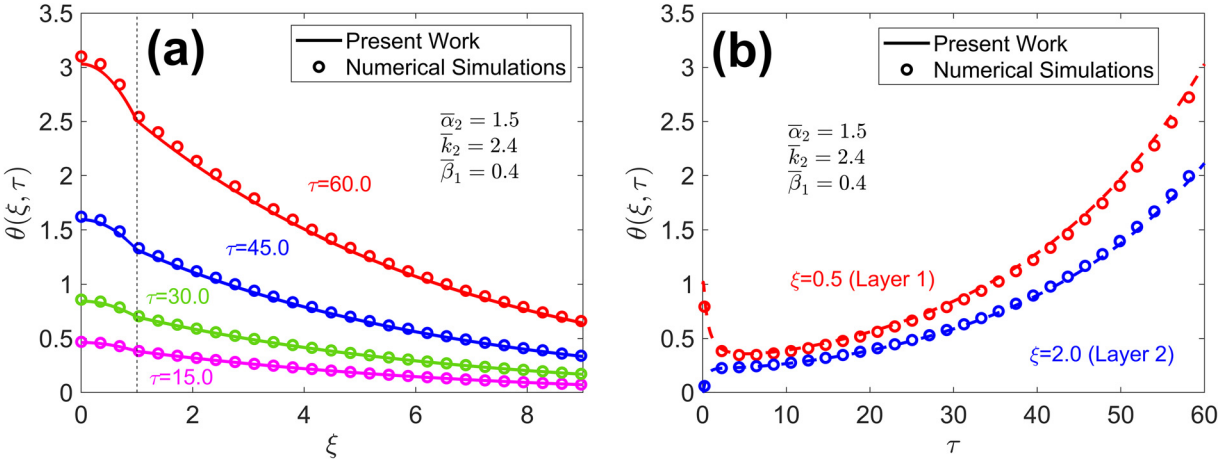

Fig. 5. Comparison with finite-element simulations: (a) Temperature distributions at multiple times, and (b) temperature at two locations as functions of time calculated using the present work for $\bar{\alpha}_2 = 1.5$, $\bar{k}_2 = 2.4$, $\bar{\beta}_1 = 0.4$. Results from a finite-element simulation are also presented for comparison.

layer as a function of time, and Fig. 4(b) presents a plot of temperature distribution in both layers at $\tau = 0.1$. In each case, curves for multiple values of $\bar{\beta}_1$ are presented, and the pure-diffusion curve based on past work [7] is also presented for comparison.

Fig. 4(a) shows greater temperature rise over time with increasing value of $\bar{\beta}_1$, which is consistent with expectations, since increasing $\bar{\beta}_1$ results in increased heat generation and thus greater temperature rise. As the value of $\bar{\beta}_1$ reduces, Fig. 4(a) shows that the temperature curves from the present work approach the pure-diffusion curve, as expected. For $\bar{\beta}_1 = 0.01$, the curves from the present work and past work are nearly identical. The temperature distributions in both layers at a specific time presented in Fig. 4(b) show, consistent with Fig. 4(a), greater temperature rise with increasing $\bar{\beta}_1$. Further, the temperature rise is always greater in the finite layer, which is also consistent with heat generation occurring in the finite thickness layer. Similar to Fig. 4(a), curves based on the present work in Fig. 4(b) approach the pure diffusion curve from past work as the value of $\bar{\beta}_1$ reduces. This shows that results from the present work correctly reduce to pure-diffusion results as the value of $\bar{\beta}_1$ reduces to zero.

In addition to comparison with past work for a special case, results from the present work are also compared with finite-element numerical simulations carried out in ANSYS. For this purpose, a one-dimensional geometry is modeled and discretized. The semi-infinite medium is simulated by considering a long enough geometry such that the temperature at the other end of the geometry can be verified to always remain close to zero within the simulated time period. Temperature-dependent heat generation in the finite layer is simulated using a user-defined function. All other aspects of the simulation are chosen to be identical to the assumptions outlined in Section 2. Grid and timestep independence of simulations is confirmed by continuing to refine the mesh and time step until further refinement does not result in significant change in the predicted temperature field. Comparison between the analytical model and finite-element simulations is carried out in terms of temperature distributions at multiple times in Fig. 5(a), and temperatures at multiple locations as functions of time in Fig. 5(b). Problem parameters are $\bar{\beta}_1 = 0.4$, $\bar{\alpha}_2 = 1.5$ and $\bar{k}_2 = 2.4$. Both plots show excellent agreement between the present work and numerical simulations over the entire geometry and throughout the time duration. The worst-case deviation between the two is found to be 1.3%, which is quite reasonable. The small deviation may arise from computational error in finite-element simulations as well as computations in the present work.

5.2. Evolution of temperature field with time

It is of interest to predict how the temperature field in the finite layer changes over time. In particular, whether the temperature field converges or diverges at large time is of much practical interest for safety design. In this case, evolution of the temperature field is governed by several physical processes that occur in parallel with each other. Firstly, heat generation within the finite layer occurs proportional to the local temperature, and, therefore, as the local temperature rises/falls, so does the heat generation rate. Further, heat diffuses within the finite layer towards the semi-infinite medium, and is then conducted into the semi-infinite medium at the interface. Further diffusion within the semi-infinite medium may increase the temperature of the semi-infinite medium, particularly close to the interface, with increasing time. This implies that the rate of heat removal by the semi-infinite medium may reduce over time due to diminished temperature difference between the two layers. In order to highlight the interplay between these various processes going on in this problem, temperature at $\xi = 0.5$ in the finite layer is plotted as a function of time for two different values of $\bar{\beta}_1$ in Fig. 6(a) and Fig. 6(b), while holding other parameters constant. For a relatively small value of $\bar{\beta}_1$, implying weak connection between heat generation rate and temperature rise, Fig. 6(a), particularly the inset within the plot, shows that temperature in the finite layer decreases at first. This is because at early times, temperature evolution is dominated by diffusion towards the semi-infinite medium, while heat generation is still quite low due to the small value of $\bar{\beta}_1$. In some time, however, the temperature reaches a minima (see inset of Fig. 6(a)), which is when heat removal into the semi-infinite medium has saturated, due to temperature rise in the semi-infinite medium, and, afterwards, heat generation within the finite layer slowly begins to become more and more significant in comparison. This results in slow temperature rise past the minima in Fig. 6(a). Over some time, significant temperature rise has occurred within the finite layer due to the increasing dominance of heat generation over diffusion. Due to the positive feedback between temperature and heat generation, eventually, the temperature curve diverges, even though it may occur after considerable time due to the relatively small value of $\bar{\beta}_1$. Such divergence even for small $\bar{\beta}_1$ is consistent with the unconditionally unstable nature of this problem, as proved in Section 4.

For comparison, a similar temperature curve is also plotted in Fig. 6(b) for a relatively larger value of $\bar{\beta}_1 = 2.0$. An inset of the temperature curve at very small times is also shown. Fig. 6(b) shows interesting changes in the temperature curve, particularly

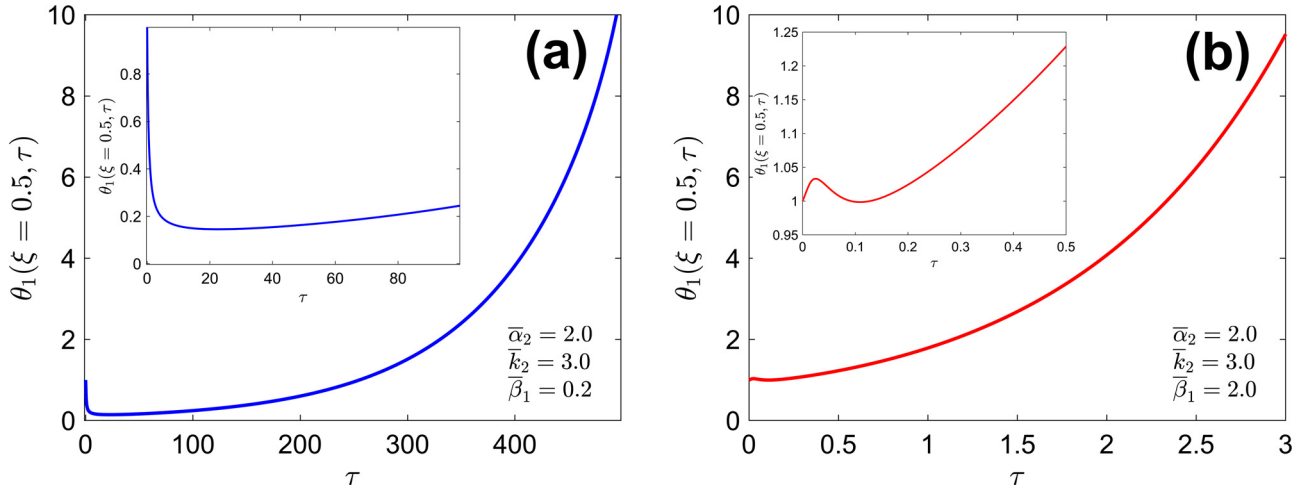

Fig. 6. Evolution of temperature at center of finite layer ($\xi = 0.5$) with time for a representative problem with (a) $\bar{\beta}_1 = 0.2$ and (b) $\bar{\beta}_1 = 2.0$. Insets show zoomed-in plots at small times. Other problem parameters are $\bar{\alpha}_2 = 2$, $\bar{k}_2$ =3.

at very small times. It is seen, particularly in the inset, that the temperature rises for a short time to reach a local maxima, then start going down to reach a minima, and then begins to monotonically rise and eventually diverge. This interesting behavior of the temperature curve may be explained on the basis of the balance between diffusion, heat removal and the diminishing role of the semi-infinite medium over time. At very early times, the thermal diffusion wave from the center of the finite layer has not yet reached the interface, and, therefore, the semi-infinite medium has very little influence. On the other hand, since the value of $\bar{\beta}_1$ is relatively large, therefore, heat generation dominates at very early times, which explains the first peak in the inset in Fig. 6(b). Once diffusion reaches the interface, some heat removal begins to occur, which results in reduction in temperature for a small time beyond the maxima. However, since $\bar{\beta}_1$ is so large, this reduction in temperature is short-lived, and heat generation soon begins to dominate the dynamics of this problem once more. The slowdown in heat removal into the semi-infinite medium due to its own temperature rise also likely contributes towards this phenomenon. Eventually, similar to the first case presented in Fig. 6(a), there is a divergence in the temperature curve for this case as well, although the divergence in the present case occurs at a much earlier time than the first case. This is explained on the basis of the much larger value of $\bar{\beta}_1$ in the second case, which results in a lot more aggressive increase in heat generation rate with temperature, resulting in divergence much earlier due to the strong positive feedback.

Fig. 7 presents temperature distributions within the finite thickness layer and semi-infinite medium at multiple times for the two cases considered above. The $\bar{\beta}_1 = 0.2$ curves presented in Fig. 7(a) show a reduction in the temperature field first at early times, followed by slow increase in the temperature field over time, eventually leading to divergence at large time. In contrast, with $\bar{\beta}_1 = 2.0$, the temperature field diverges much faster, and at each time plotted here, the finite layer is much hotter than the semi-infinite medium, compared to the $\bar{\beta}_1 = 0.2$ case. In each of the cases plotted in Fig. 7(a) and Fig. 7(b), the temperature curve is flat at $\xi = 0$, consistent with symmetry considerations, and the temperature field in the semi-infinite medium far away from the interface approaches zero, also consistent with the semi-infinite nature of the medium. There is continuity of the temperature field at the interface, but the slopes are different, which is due to the different values of thermal conductivity of the two materials.

The proof presented in Section 4 establishes unconditional instability of this problem regardless of how small $\bar{\beta}_1$ is, as long as

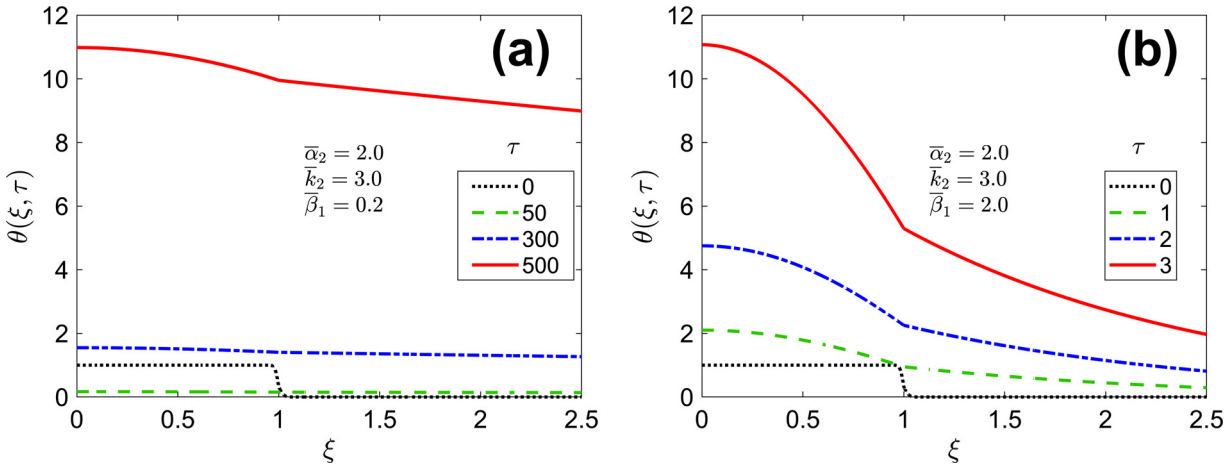

Fig. 7. Evolution of temperature distribution in the two layers at multiple times for a representative problem with $\bar{\alpha}_2 = 2$, $\bar{k}_2$ =3. Plots are presented for (a) $\bar{\beta}_1 = 0.2$ and (b) $\bar{\beta}_1 = 2.0$.

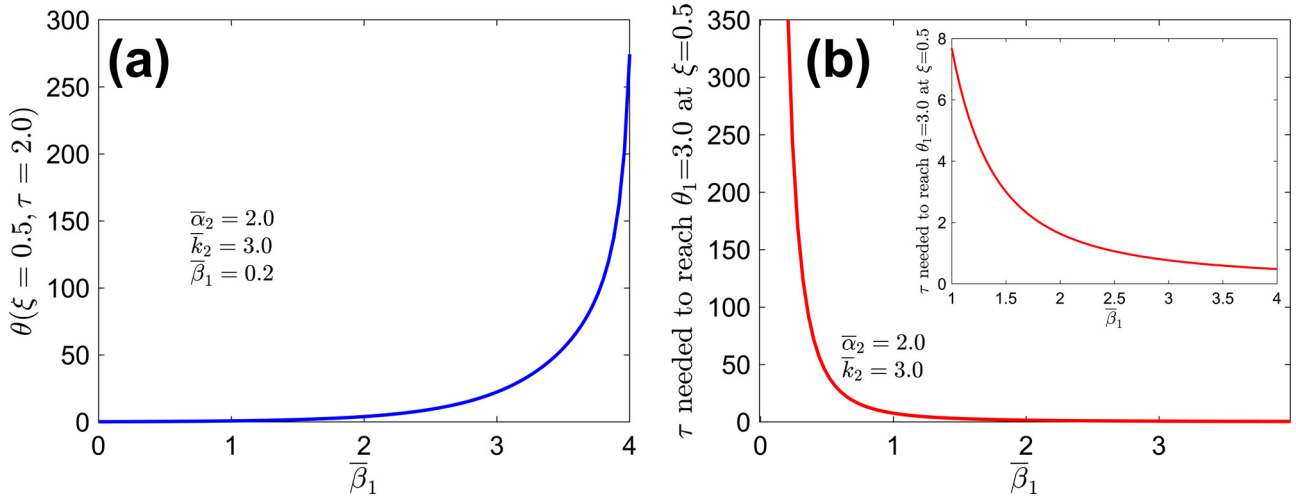

Fig. 8. Effect of heat generation coefficient: (a) Temperature at the center of the finite layer ($\xi = 0.5$) at $\tau = 2$, and (b) time taken for temperature at the center of the finite layer to reach θ_1=3.0, both plotted as functions of $\bar{\beta}_1$. Other problem parameters are $\bar{\alpha}_2 = 2$, $\bar{k}_2$ =3.

$\bar{\beta}_1 > 0$. The divergence predicted by the proof is seen for both values of $\bar{\beta}_1$ presented in Figs. 6 and 7. However, it is important to note that such divergence occurs over very different time periods, depending on the value of $\bar{\beta}_1$. Since practical heat-generating processes occur only for a specific time period, therefore, the temperature field in a practical device may remain bounded within the time period of interest, despite the unconditional instability at large times proved here.

5.3. Impact of heat generation coefficient

Since the heat generation coefficient $\bar{\beta}_1$ is an important parameter in this problem, further investigation of the effect of $\bar{\beta}_1$ on the temperature distribution is carried out. In practical problems, $\bar{\beta}_1$ is determined on the basis of the physical processes responsible for temperature-dependent heat generation. For example, in the case of a Li-ion cell, chemical decomposition reactions within the cell generate heat, and the nature of these reactions helps determine the value of $\bar{\beta}_1$ [14,30]. As another example, in the case of thermal runaway in a MOSFET, the strength of the underlying temperature dependence of current can be used to determine $\bar{\beta}_1$ [15]. Such practical problems are also often governed by a specific time interval of interest, which in these examples may be the total charge/discharge time for a Li-ion cell or the pulse width of the MOSFET, respectively. Further, each of these devices are characterized by a maximum tolerable temperature, on the basis of performance, safety and reliability considerations. Therefore, it is of interest to examine the interplay between $\bar{\beta}_1$ and the operating parameters outlined above.

Fig. 8(a) plots the temperature at the center of the finite layer (ξ=0.5) at the end of a particular time period, τ=2.0, as a function of time heat generation coefficient $\bar{\beta}_1$. As expected, there is a strong dependence of the temperature rise on $\bar{\beta}_1$. In general, there is small temperature rise for low values of $\bar{\beta}_1$, but the temperature increases exponentially for larger values. The strong dependence shown by Fig. 8(a) highlights the importance of keeping $\bar{\beta}_1$ as low as possible in practical systems in order to minimize the risk of thermal runaway.

Note that Fig. 8(a) is plotted at a specific time, whereas, it is possible that the total time interval of practical systems may be governed by other considerations. Therefore, the time taken for temperature at the center of the finite layer to reach a threshold value, say, $\theta_{max} = 3$ is calculated as a function of $\bar{\beta}_1$. If the actual time period of the process is lower than this calculated threshold, then the layer temperature will stay below θ_{max}, whereas, the actual time period being greater would indicate unacceptably large temperature rise within the process. This plot is presented in Fig. 8(b), which indicates a rapid increase in the time taken to reach θ_{max} as $\bar{\beta}_1$ reduces. This indicates the capability to withstand the temperature-dependent heat generation for longer and longer time as $\bar{\beta}_1$ decreases, which is along expected lines. The time taken to reach θ_{max} is extremely large for sufficiently small values of $\bar{\beta}_1$, even though, Section 4 shows that the system is unstable for any positive $\bar{\beta}_1$. Therefore, depending on how long an actual process lasts and the maximum temperature that can be tolerated, the system can still survive, despite the unconditional instability. Note that due to the sharp increase in the time taken to reach θ_{max} at small values of $\bar{\beta}_1$, a plot is provided as an inset in order to show this curve between $\bar{\beta}_1 = 1$ and $\bar{\beta}_1 = 4$, which shows, as expected a continued reduction in time taken to reach θ_{max} as $\bar{\beta}_1$ increases.

In some applications, the average temperature of the finite layer may also be of interest. Fig. 9 plots this quantity as a function of time for different values of $\bar{\beta}_1$, with other parameters held constant at $\bar{\alpha}_2 = 2.0$ and $\bar{k}_2 = 3.0$. Since the temperature field diverges for these cases, the plot is cut off at a maximum temperature value

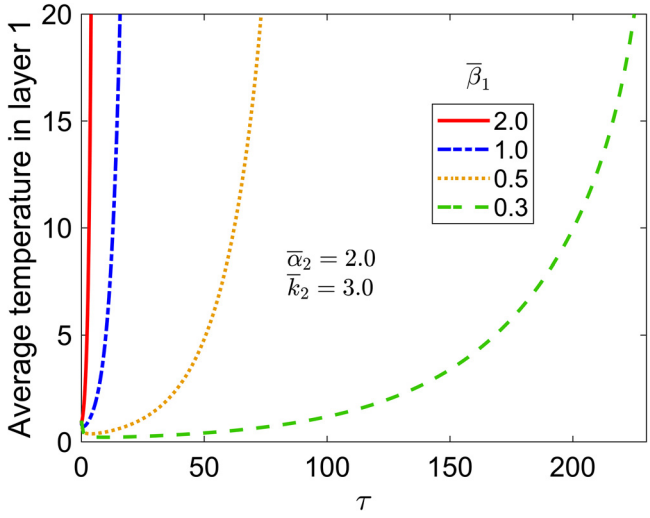

Fig. 9. Effect of heat generation coefficient: Average temperature in the finite thickness layer as a function of τ at multiple values of $\bar{\beta}_1$. Other problem parameters are $\bar{\alpha}_2 = 2$, $\bar{k}_2$ =3.

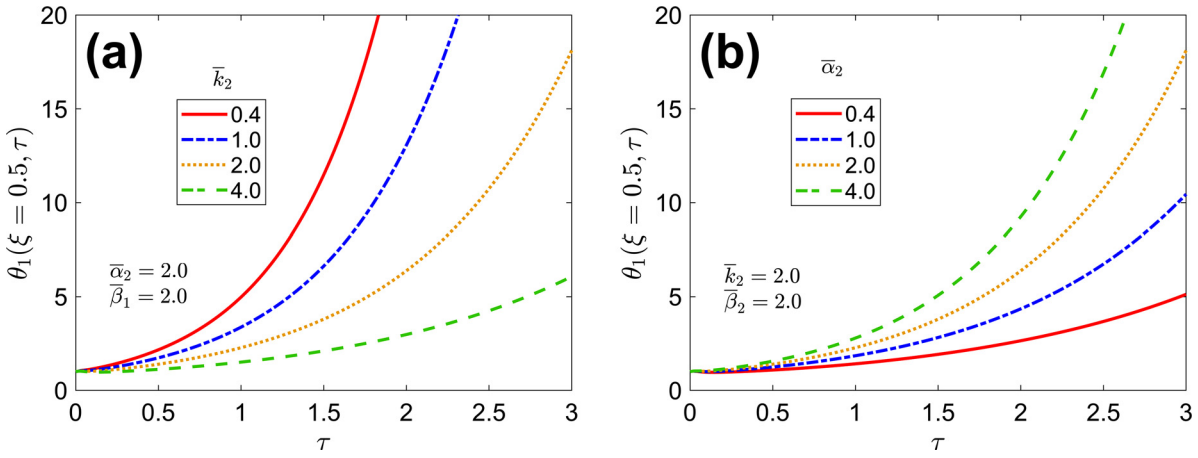

Fig. 10. Effect of thermal properties of the semi-infinite medium: Temperature at the center of layer 1 as a function of time for multiple values of (a) $\bar{k}_2$ and (b) $\bar{\alpha}_2$, for $\bar{\beta}_1 = 2$. In parts (a) and (b), $\bar{\alpha}_2 = 2$ and $\bar{k}_2 = 2$, respectively.

of 20. Fig. 9 shows that the average temperature of the finite layer always diverges, although for small values of $\bar{\beta}_1$, divergence is relatively slow and the rapid rise in temperature is preceded by a long period in which temperature does not change much. In contrast, for larger values of $\bar{\beta}_1$, such as $\bar{\beta}_1 = 2.0$, the average temperature begins to go up almost immediately and rises very rapidly. The time taken to reach a temperature value of 20 is about 57 times larger for $\bar{\beta}_1 = 2.0$ than for $\bar{\beta}_1 = 0.2$.

5.4. Effect of thermal properties

Thermal properties of the two materials clearly play an important role in determining the nature of the temperature distribution. Of particular interest is the thermal conductivity and thermal diffusivity of the semi-infinite medium, relative to the finite layer. For example, a number of materials are available for cooling of a Li-ion cell, and it is important to benchmark the thermal performance of candidate materials. Fig. 10(a) and Fig. 10(b) present curves for temperature at ξ=0.5 in the finite layer as a function of time for different values of $\bar{k}_2$ and $\bar{\alpha}_2$, respectively, while other thermal properties are held constant. Results indicate strong influence of both $\bar{k}_2$ and $\bar{\alpha}_2$ on temperature distribution. As $\bar{k}_2$ increases, Fig. 10(a) shows that temperature rise in the finite layer becomes smaller and smaller. Even though each curve is expected to diverge eventually, in practical problems, the lower rate of growth of temperature for large $\bar{k}_2$ implies greater time window available for the heat generation process (such as discharge of a Li-ion cell or operation of a MOSFET device) to complete. The strong dependence of temperature on $\bar{k}_2$ is not surprising, since $\bar{k}_2$ is the primary thermal property that governs interfacial heat transfer from the finite layer into the semi-infinite medium, per Eq. (13). On the other hand, Fig. 10(b) shows that increasing $\bar{\alpha}_2$ results in greater temperature rise. This is because a larger value of $\bar{\alpha}_2$, while holding $\bar{k}_2$ constant, is equivalent to lower volumetric heat capacity, which results in greater temperature rise in the semi-infinite medium, thus lower heat removed from the finite layer and, therefore, greater temperature rise in the finite layer. Note that in practical materials, thermal conductivity and diffusivity usually both rise/fall together, which is why, it may be more appropriate to carry out such analysis while letting both properties vary. This has been presented in the next sub-section for materials of practical interest.

5.5. Practical design guidelines

The theoretical results presented in this work can be helpful in the design and optimization of practical engineering systems. For example, it is of interest to determine $\bar{\beta}_{1,max}$, the highest heat generation coefficient that can be tolerated over a time interval τ_{total} without the peak temperature exceeding a desired threshold. This problem is first addressed in non-dimensional form in order to produce universal design curves, and then applied to a specific practical problem related to thermal design of Li-ion cells.

Fig. 11 plots $\bar{\beta}_{1,max}$ as a function of τ_{total}, the total time taken by the process for given thermal properties ($\bar{\alpha}_2 = 2.0$, $\bar{k}_2 = 3.0$). Plots are presented for four different values of the peak temperature θ_{max}. Fig. 11 shows that the larger the value of τ_{total}, i.e., the longer the heat generation occurs, the larger is the risk of exceeding θ_{max}, and, therefore, the smaller is the maximum heat generation coefficient that can be tolerated. However, in each case shown in Fig. 11, there is a plateau effect, in that there is a sharp reduction in $\bar{\beta}_{1,max}$ when τ_{total} is small, but for larger values, the impact on $\bar{\beta}_{1,max}$ is much less significant. Fig. 11 also shows that the larger the value of θ_{max}, the larger is the value of $\bar{\beta}_{1,max}$. A large value of θ_{max} allows a relaxed thermal design, since a large temperature peak can be tolerated. Therefore, a larger value of $\bar{\beta}_{1,max}$ can be accommodated compared to when θ_{max} is small, in which case, even small $\bar{\beta}_{1,max}$ can cause sufficient temperature rise to exceed the threshold.

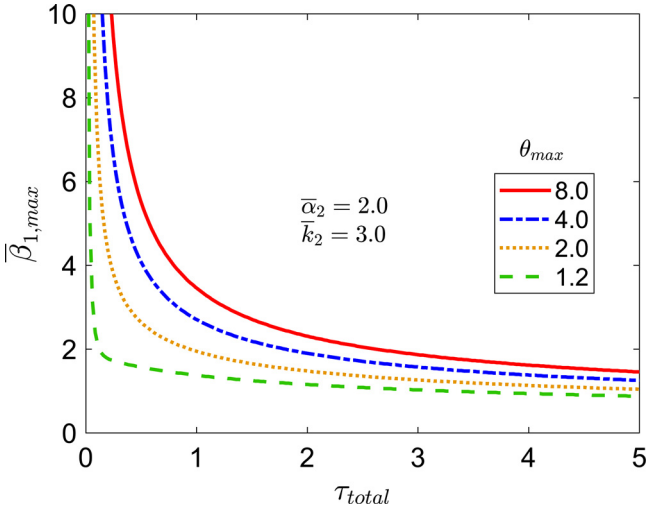

Fig. 11. Maximum heat generation coefficient $\bar{\beta}_1$ in order to keep the peak temperature below a threshold θ_{max} as a function of time duration of heat generation. Curves are plotted for several values of θ_{max}. Other parameters are $\bar{\alpha}_2 = 2.0$, $\bar{k}_2 = 3.0$.

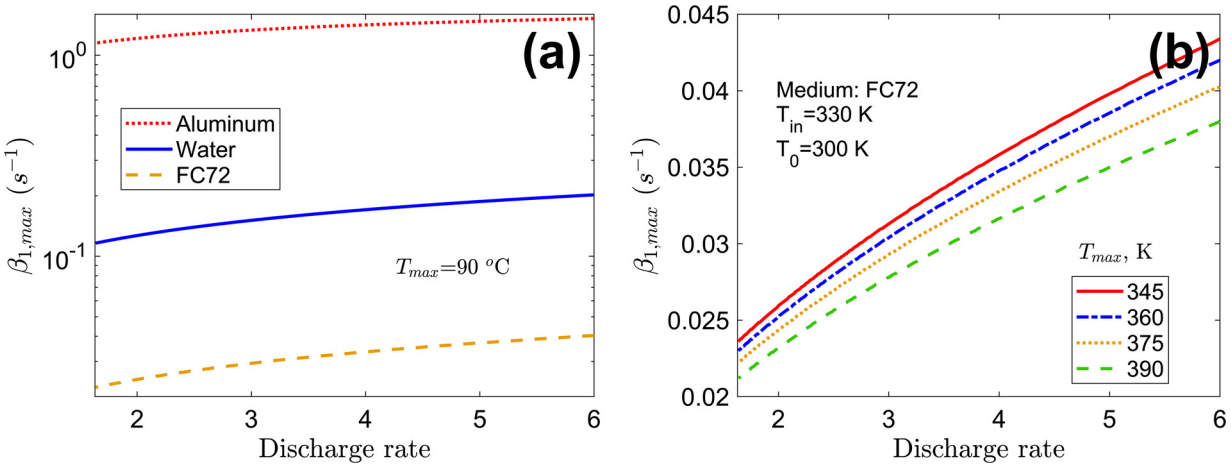

Fig. 12. Applications for Li-ion battery thermal design: (a) Maximum tolerable heat generation coefficient β_1 as a function of discharge time represented by the discharge rate in order to keep the peak temperature below 360 K. Curves are plotted for three different materials around the cell. (b) Maximum tolerable heat generation coefficient β_1 as a function of discharge rate for different values of highest permissible peak temperature. Curves correspond to FC72 material around the cell. In both cases, the ambient is at 300 K and the initial temperature of the cell is 330 K.

Fig. 11 is presented in completely non-dimensional form to facilitate its use as a universal design tool for any general system regardless of specific dimensions or thermal properties. The use of plots similar to Fig. 11 for solving a practical engineering problem is illustrated in the context of a prismatic Li-ion cell being cooled in a large surrounding ambient. In order to prevent thermal runaway of a Li-ion cell, the cell temperature is required to be maintained below a certain threshold [14,31]. This requires effective dissipation of heat generated within the cell due to temperature-dependent decomposition reactions.

In the context of a Li-ion cell, the C-rate, also known as discharge rate characterizes the time duration of a discharge process [32]. The C-rate of a discharge process is defined as the reciprocal of the number of hours taken for the process to completely discharge the cell, starting from a fully charged cell [32]. For example, C-rates of 1C and 4C correspond to a total discharge time of 1 h and 0.25 h, respectively. Starting from an initial temperature of the cell, it is of interest to determine if, for a given C-rate of the discharge process, the cell temperature will exceed the threshold temperature before the process is complete. If the threshold temperature is not exceeded before the process is complete, the cell will not undergo thermal runaway despite the unconditional instability of the process proved in Section 4 above, because once the process is complete, there is no longer any heat generation and the cell can begin to cool down.

Two specific questions related to diffusion-reaction heat transfer in a discharging Li-ion cell surrounded by a large medium are answered using the model. Firstly, the performance of three different materials around the Li-ion cell is characterized and compared. For a 10 mm thickness cell initially at 330 K with an ambient temperature of 300 K, the maximum value of heat generation coefficient, $\beta_{1,max}$ is computed for different C-rates. Three different materials around the cell – FC72, which is a dielectric fluid [33], water and Aluminum – are considered. While FC72 and water may be used for immersion cooling, in some applications, the cell is packaged within an Aluminum matrix. Thermal properties of the Li-ion cell are taken from past measurements on an 18650 cell [34,35]. Standard thermal properties are assumed for water and Aluminum. Properties for FC72 are obtained from manufacturer datasheet [33].

Results pertaining to this materials comparison are presented in Fig. 12(a) and Fig. 12(b). These data show significant difference in thermal performance of the device depending on the nature of the medium around the cell. In case of FC72, due to its relatively poor thermal properties, the maximum tolerable value of $\beta_{1,max}$ is quite small. Due to superior thermal properties, water performs better and Aluminum even better. As expected, the greater the discharge rate, i.e., shorter the time duration of the discharge process, and therefore, the greater is the value of $\beta_{1,max}$ that can be targeted without exceeding the threshold temperature. Fig. 12(b) shows, as expected, that for a given coolant material, as the discharge goes up, the maximum tolerable value of heat generation also goes up. Further, as the threshold temperature becomes more and more stringent, the maximum tolerable value of heat generation reduces. Note that for thermal properties corresponding to a Li-ion cell [34,35], a value of $\beta_{1,max} = 0.01$ s^{-1} corresponds to a dQ'''/dT value of around 16,500 Wm^{-3}K^{-1}, where Q''' is the volumetric heat generation rate.

6. Conclusions

The key contributions of this work include the development of a theoretical model for understanding multilayer diffusion-reaction in a problem where one layer is finite and the other is semi-infinite, as is commonly encountered in battery cooling, MOSFET device thermal performance and related problems. The theoretical proof of unconditional instability of this problem presented here contributes towards extending the state-of-the-art in the theory of thermal stability, particularly since there is only limited literature on thermal stability analysis using the Laplace solution [36].

While these theoretical results indicate that this problem is, in principle, unconditionally unstable, results also indicate that the temperature of the finite layer may actually reduce for some time before diverging. It is also shown that the time taken for divergence may be quite large under certain conditions, for example when the heat generation coefficient is small. Therefore, despite the unconditionally unstable nature of the problem, practical diffusion-reaction processes may still remain within a reasonable thermal envelope if the time duration of the process is reasonably short.

Non-dimensional curves, such as those presented in Fig. 11 may serve as universal design tools, regardless of the specific values of dimensions and other parameters of a specific problem, and, therefore, may be used for a wide variety of applications. One specific application discussed in this work – cooling of a Li-ion cell during discharge – may be of particular relevance for ensuring safe electrochemical energy conversion and storage.

It is important to recognize the key limitations and assumptions underlying the present work. The heat generation phenomenon has been linearized, as is commonly the case for first-order analysis [14,18,19]. All thermal properties are assumed to remain constant, despite change in temperature. Natural convection heat transfer or any other fluid flow in the surrounding medium has been neglected. In case the surrounding medium is a fluid, it is important to confirm the validity of this assumption by confirming that the governing Rayleigh number is sufficiently small.

Declaration of Competing Interest

The author declares that there are no competing interests in connection with the work presented here.

CRediT authorship contribution statement

Ankur Jain: Conceptualization, Methodology, Formal analysis, Validation, Investigation, Data curation, Project administration, Writing – original draft, Writing – review & editing.

Data availability

Data will be made available on request.

Acknowledgments

This material is based upon work supported by CAREER Award No. CBET-1554183 from the National Science Foundation.

References

[1] S.E. Gustafsson, Transient plane source techniques for thermal conductivity and thermal diffusivity measurements of solid materials,', Rev. Sci. Instrum. 62 (1991) 797, doi:10.1063/1.1142087.
[2] M. Emanuel, Effusivity Sensor Package (ESP) system for process monitoring and control, in: Proceedings of the 28th International Thermal Conductivity Conference, 2022. St. Andrews by-the-Sea, NB, Canada Available at https://memanuel.files.wordpress.com/2010/08/mathis_effusivity_sensor_technology3.pdf last accessed 10/17/2022.
[3] K. Daryabeigi, Thermal analysis and design optimization of multilayer insulation for reentry aerodynamic heating, J. Spacecr. Rocket. 39 (2002) 509–514, doi:10.2514/2.3863.
[4] D.H. Kang, S. Lorente, A. Bejan, Constructal distribution of multi-layer insulation, Int. J. Energy Res. 37 (2013) 153–160, doi:10.1002/er.1895.
[5] P. Hui, H.S. Tan, A transmission-line theory for heat conduction in multilayer thin films, IEEE Trans. Compon. Packag. Manufac. Technol. Part B 17 (1994) 426–434, doi:10.1109/96.311793.
[6] M. Cavalcante, S. Marques, M.J. Pindera, Transient thermomechanical analysis of a layered cylinder by the parametric finite-volume theory, J. Thermal Stresses 32 (2008) 112–134,, doi:10.1080/01495730802540783.
[7] D.W. Hahn, M.N. Özışık, Heat Conduction, Section 10.7, 3rd ed., Wiley, Hoboken, N.J., 2012 ISBN: 978-0-470-90293-6.
[8] C.W. Tittle, Boundary value problems in composite media: quasi-orthogonal functions, J. Appl. Phys. 36 (1965) 1486–1488, doi:10.1063/1.1714335.
[9] Y. Yener, M.N. Özışık, On the solution of unsteady heat conduction in multi-region media with time-dependent heat transfer coefficient, in: Proceedings of the 5th International Heat Transfer Conference, Tokyo, Japan, 1974, pp. 188–192.
[10] L. Zhou, M. Parhizi, A. Jain, Theoretical modeling of heat transfer in a multilayer rectangular body with spatially-varying convective heat transfer boundary condition,', Int. J. Therm. Sci. 170 (2021) 107156, doi:10.1016/j.ijthermalsci.2021.107156.
[11] E.J. Carr, I.W. Turner, A semi-analytical solution for multilayer diffusion in a composite medium consisting of a large number of layers, Appl. Math. Model. 40 (2016) 7034–7050, doi:10.1016/j.apm.2016.02.041.
[12] C.H. Wang, X.Y. Zhang, Z.Y. Jiang, Discontinuous finite element method for transient conductive heat transfer in layered media with thermal contact resistance, Int. Commun. Heat Mass Transf. 138 (2022) 106344, doi:10.1016/j.icheatmasstransfer.2022.106344.
[13] H.T. Chen, J.Y. Lin, Numerical analysis for hyperbolic heat conduction, Int. J. Heat Mass Transf. 36 (1993) 2891–2898, doi:10.1016/0017-9310(93)90108-I.
[14] K. Shah, D. Chalise, A. Jain, Experimental and theoretical analysis of a method to predict thermal runaway in Li-ion cells, J. Power Sources 330 (2016) 167–174, doi:10.1016/j.jpowsour.2016.08.133.
[15] P. Spirito, G. Breglio, V. d'Alessandro, N. Rinaldi, Analytical model for thermal instability of low voltage power MOS and S.O.A. in pulse operation, in: Proceedings of the 14th International Symposium on Power Semiconductor Devices & ICs, 2002, doi:10.1109/ISPSD.2002.1016223.
[16] S. Mcginty, A decade of modelling drug release from arterial stents, Math. Biosci. 257 (2014) 80–90, doi:10.1016/j.mbs.2014.06.016.
[17] G. Krishnan, M. Parhizi, M. Pathak, A. Jain, Solution phase limited diffusion modeling in a Li-ion cell subject to concentration-dependent pore wall flux, J. Electrochem. Soc. 168 (2021) 090511, doi:10.1149/1945-7111/ac1cfb.
[18] A. Jain, M. Parhizi, L. Zhou, G. Krishnan, Imaginary eigenvalues in multilayer one-dimensional thermal conduction problem with linear temperature-dependent heat generation, Int. J. Heat Mass Transf. 170 (2021) 120993 1–10, doi:10.1016/j.ijheatmasstransfer.2021.120993.
[19] A. Jain, M. Parhizi, L. Zhou, Multilayer One-Dimensional Convection-Diffusion-Reaction (CDR) Problem: analytical Solution and Imaginary Eigenvalue Analysis,', Int. J. Heat Mass Transf. 177 (2021) 121465 1–11, doi:10.1016/j.ijheatmasstransfer.2021.121465.
[20] N. Rinaldi, On the modeling of the transient thermal behavior of semiconductor devices, IEEE. Trans. Electron. Dev. 48 (2001) 2796–2802, doi:10.1109/16.974706.
[21] D. Frank-Kamenetskii, Diffusion and Heat Exchange in Chemical Kinetics, Princeton University Press, 2015.
[22] G. Krishnan, A. Jain, Derivation of multiple but finite number of imaginary eigenvalues for a two-layer diffusion-reaction problem, Int. J. Heat Mass Transf. 194 (2022) 123037 1-7, doi:10.1016/j.ijheatmasstransfer.2022.123037.
[23] S.S. S.alvi, A. Jain, A review of recent research on heat transfer in three-dimensional integrated circuits (3-D ICs), IEEE Trans. Compon. Packag. Manuf. Technol. 11 (2021) 802–821, doi:10.1109/TCPMT.2021.3064030.
[24] A.K. Henning, B. Rajendran, B. Cronquist, Z. Or-Bach, Thermal considerations for monolithic integration of three-dimensional integrated circuits, in: Proceedings of the IEEE SOI-3D-Subthreshold Microelectronics Technology Unified Conference, 2013, doi:10.1109/S3S.2013.6716559.
[25] S. Oss, A simple model of thermal conduction in human skin: temperature perception and thermal effusivity, Eur. J. Phys. 43 (2022) 035101, doi:10.1088/1361-6404/ac4c8a.
[26] F.R. de Hoog, J.H. Knight, A.N. Stokes, An improved method for numerical inversion of Laplace transforms, SIAM J. Sci. Stat. Comput. 3 (1) (1982), doi:10.1137/0903022.
[27] A. Talbot, The accurate numerical inversion of Laplace transforms, IMA J. Appl. Math. 23 (1979) 97–120, doi:10.1093/imamat/23.1.97.
[28] K.L. Hitz, T.E. Fortmann, An Introduction to Control Systems, CRC Press, 1977 ISBN: 978-0824765125.
[29] J.H. Mathews, R.W. Howell, Complex Analysis for Mathematics and Engineering, 6th Ed., Jones & Bartlett Learning, 2011 ISBN: 978-1449604455.
[30] I. Esho, K. Shah, A. Jain, Measurements and modeling to determine the critical temperature for preventing thermal runaway in Li-ion cells, Appl. Thermal Eng. 145 (2018) 287–294, doi:10.1016/j.applthermaleng.2018.09.016.
[31] J. Weng, Q. Huang, X. Li, G. Zhang, D. Ouyang, M. Chen, A. Yuen, A. Li, E. Lee, W. Yang, J. Wang, X. Yang, Safety issue on PCM-based battery thermal management: material thermal stability and system hazard mitigation, Energy Storage Mater. 53 (2022) 580–612, doi:10.1016/j.ensm.2022.09.007.
[32] J. Newman, K.E. Thomas-Alyea, Electrochemical Systems, 3rd Ed., Wiley-Interscience, 2004 ISBN: 978-0471477563.
[33] Technical Data: 3M™ Fluorinert™ Electronic Liquid FC-72, available at https://multimedia.3m.com/mws/media/648920/3m-fluorinert-electronic-liquid-fc72-en.pdf, last accessed 11/02/2022.
[34] S. Drake, D. Wetz, J. Ostanek, S. Miller, J. Heinzel, A. Jain, Measurement of anisotropic thermophysical properties of cylindrical Li-ion cells, J. Power Sources 252 (2014) 298–304, doi:10.1016/j.jpowsour.2013.11.107.
[35] M. Ahmed, S. Shaik, A. Jain, Measurement of radial thermal conductivity of a cylinder using a time-varying heat flux method, Int. J. Therm. Sci. 129 (2018) 301–308, doi:10.1016/j.ijthermalsci.2018.03.008.
[36] B. Yang, H. Shi, A thermal stability criterion for heat conduction in multilayer composite solids, J. Heat Tranf. 131 (2009) 111301–111304 7, doi:10.1115/1/3153581.